Article:
Bryant, M orcid.org/0000-0003-4442-5169, Sin, JR, Emami, N et al. (1 more author) (2020) Effect of proteins and phosphates on the degradation and repassivation of CoCrMo alloys under tribocorrosion conditions. Tribology - Materials, Surfaces & Interfaces, 14 (4). pp. 207-218. ISSN 1751-5831

https://doi.org/10.1080/17515831.2020.1746012

Effect of proteins and phosphates on the degradation and repassivation of CoCrMo alloys under tribocorrosion conditions

M. Bryant[1], J. Rituerto Sin[2], S. Suñer[2], N. Emami[2] and A. Neville[1]

[1]Institute of Functional Surface, University of Leeds, Leeds, LS2 9JT UK

[2]Division of Machine Elements, Luleå University of Technology, Luleå, SE-971 87 Sweden

Abstract

Cobalt-chromium-molybdenum alloys are commonly used for biomedical applications such as dental implants and joint implants. Once the material is implanted into the body it is exposed to the corrosiveness of biological fluids and, in some cases, to mechanical loading that can lead to the combined action of wear and corrosion; better known as tribocorrosion. The chemical composition of the media where the material is immersed can affect the tribocorrosion processes that take place. The effect of four different simulated body fluids on the tribocorrosion behaviour of a CoCrMo alloy has been investigated. The degradation of the studied CoCrMo alloys due to tribocorrosion phenomena shows a great dependence on the chemical composition of the media. It has been observed that PBS-based solutions tend to show higher mass loss than the solutions prepared with distilled water. Phosphates present in PBS tend to accumulate on the surface of the alloy and change its tribological performance. In addition, proteins show a lubricating effect reducing the coefficient of friction of the system in the boundary lubrication regime.

Keywords: tribocorrosion, CoCrMo alloy, PBS, simulated body fluid.

1. Introduction

The good corrosion and wear resistance of cobalt chromium alloys often make them the material of choice for various biomedical applications such as stents, dental implants and joint implants [1-3]. The high corrosion resistance of these alloys is owed to the spontaneous formation of a protective oxide layer on the surface, which is primarily composed by chromium oxide (Cr_2O_3) [4]. However, the oxide layer can be disrupted if the material is subject to mechanical loading and relative motion with hard surfaces. Breakage of the oxide layer can leave the base material unprotected and exposed to the corrosive environment, which leads to increased corrosion and release of metallic ions into to the surrounding fluids. The release of metallic ions into human body fluids can lead to a number of adverse body reactions such as the formation of pseudotumours, possible genetic effects and hypersensitivity [5].

The composition and characteristics of the oxide film affect the wear and the corrosion behaviour of the material [6]. In addition, the chemical composition of the surrounding media also has an influence on the processes of wear and corrosion [7]. The study of the effect of the adsorption of albumin on CoCrMo alloy under static conditions has shown a double side effect [8]. On one hand, proteins can act as a barrier blocking the access of oxidants to the metal surface and effect mass transportation processes. On the other hand, proteins can bind with metallic ions, which increases the dissolution rate of the material. Studies of the corrosion of CoCrMo alloys have also shown that albumin can increase the release of Mo ions in static corrosion conditions [7]. In addition to the effect of proteins, the presence of phosphate ions in the solution also affects the corrosion behaviour of CoCrMo alloys. Phosphate ions have been shown to inhibit the anodic reactions under static corrosion conditions [8]. The competition between proteins and phosphates to adsorb on the surface of the material will inevitably affect its corrosion behaviour.

When CoCrMo alloys are exposed to tribocorrosion conditions, the nature of the lubricant also affects the performance of the metal. The lubricating effect of proteins has been previously reported by several authors [9-11]. The ability of proteins to adsorb onto CoCrMo surfaces

leads to the formation of proteinaceous films that can hypothetically reduce adhesive wear [12,13]. In the case of metal on metal hip implants, the formation of a carbon rich layer derived from proteins has been reported [13-15]. Some studies have reported signs of a graphitic structure within the carbonaceous layer [15]; the mechanisms of which are unclear. It has been shown that the presence of albumin in the environment can also increase the release of Cr and Mo under tribocorrosion conditions [7]. In the case of phosphate ions, they have shown an effect limiting dissolution of the metal exposed to wear-corrosion conditions under dynamic polarisation tests [8].

Although it is clear that the chemical composition of the lubricant affects not only the corrosion but also the tribocorrosion behaviour of CoCrMo alloys, there are various solutions commonly used in laboratory testing to simulate body fluids [16-19]. The goal of this study is to understand how the composition of the lubricant affects the tribocorrosion performance, the nature of the debris produced and the effects on re-passivation kinetics of a low carbon CoCrMo alloy. Attention is given to the effect of the proteins contained in bovine serum and phosphates.

2. Materials and Methodology

2.1. Materials

A low carbon CoCrMo alloy conforming to ASTM 1537 was studied in this work. Plates of Ø 25 mm diameter and 6 mm thickness were machined from the starting rod. Samples were ground using SiC paper up to 1200 grit. Final surface finish was achieved by polishing using diamond paste solutions of 9 µm and 3 µm. Samples were thoroughly rinsed with ethanol and distilled water between each step. Samples were immersed in ethanol and cleaned in an ultrasonic bath that allowed removal of impurities from the polishing process. Samples were finally rinsed in distilled water and assembled in the tribo-electrochemical cell.

The four electrolyte solutions used in this study are listed in Table 1. Isotonic saline solution (0.9% NaCl) and Dulbecco's phosphate-buffered solution (Sigma-Aldrich, Germany) were the

two saline solutions studied in this work. In addition, two serum solutions were prepared using bovine calf serum (Haram Sera-Lab®, UK). The first solution consisted of 25v% bovine calf serum and 75v% distilled water. The second solution consisted of 25v% bovine calf serum and 75v% phosphate buffered solution.

2.2. Tribocorrosion simulation

A ball on flat reciprocating tribometer, detailed in previous publications [10,20], was integrated with a three-electrode electrochemical cell. The electrochemical cell consisted of the tested sample used as the working electrode, a Ag/AgCl (3M KCl) electrode used as the reference electrode and a Pt wire used as the counter electrode. A silicon nitride ball of Ø = 12 mm diameter was rubbed against the CoCrMo plates at a frequency of 1 Hz during 3600 s. A normal load of 40 N was applied, which corresponds to an initial mean Hertzian pressure of 1 GPa. A stroke length of 10 mm was used.

A computer controlled potentiostat (PGSTAT101, Autolab, NV) was used to control the potential and monitor changes in electrochemical current during the tribological tests. Potentiostatic polarisation was used to simulate corrosion at an applied anodic potential of 0, 0.2 and 0.4 V vs Ag/AgCl. First, samples were immersed in the solution at open circuit potential allowing the surface to equilibrate over 1hr. Second, samples were polarised from the OCP to the selected potential. Once the required potential was reached, it was maintained in static conditions for 1800 s. After that, the tribological test was started and run for 3600 s. After sliding, the electrochemical current was monitored for a further 1800 s.

The total damage caused by tribocorrosion (T) processes are often considered as a combination of wear damage (W), corrosion damage (C) and the synergies between wear-corrosion (Wc) and corrosion-wear (Cw) [21], as shown in Equation (1). It must be noted that this equation was developed for erosion-corrosion systems at equilibrium conditions; not at an applied over-potential which is the case in this study. In this study the mechanistic approach,

outlined by Uhlig et al, was to evaluate degradation mechanisms shown in Equation (2) considering that synergistic factors will still contribute to the M_{mech} and M_{chem} variables.

$$T = M_{mech} + M_{chem} \quad (1)$$

$$M_{mech} = W + W_c \text{ and } M_{chem} = C + C_w$$

$$m = \left(\frac{Q}{F}\right)\left(\frac{M}{z}\right) \quad (2)$$

Faraday's Law (Equation 2) has been used in order to estimate the total electrochemical losses (C+Cw), which are shown in Figure 3 (a). The mass loss caused by electrochemical reactions (C+Cw) is represented by m; Q is the total electrochemical charge calculated which is calculated integrating the current measured during the potentiostatic tests with respect to time; F is the Faraday constant (96485 C/mol); M is the molar mass (58.7 g/mol) of the material and z is the valence number of the released ions (valence of oxidation was assumed 2.3). To calculate the degradation contributions, electrochemical loss ($C+C_w$) was subtracted from the total volume loss (T) measured gravimetrically and converted to mass to estimate the addition of wear and corrosion induced wear losses ($W+W_c$).

2.3. Post surface and solution analysis

After each test the coupon was removed, lightly cleaned with deionised water to remove any loose surface deposits and dried with an N_2 air stream. Mass loss was gravimetrically determined by weighing the specimens before and after each test using an micro-balance. Vertical scanning interferometry (VSI) and scanning electron microscopy (SEM) were further used to analyse the characteristics of the wear track after the tribocorrosion tests.

Samples of lubricant were collected after each test to analyse the particles formed during the tribocorrosion tests and were analysed via Nanoparticle Tracker Analysis (NTA) (Nanosight Ltd., UK). Prior to NTA, lubricant samples were dissolved in distilled water by centrifuging 3 ml to deposit the heavier metallic particles, removing 2 ml of supernatant, adding 2 ml of distilled

water, and finally immersing in a ultrasonic bath to disperse the particles in the media. This process was repeated five times.

Statistical analysis was performed to determine significant differences in the friction coefficient and the total tribocorrosion loss of CoCrMo in the fluids investigated. One-way ANOVA and the Tukey method were used ($P<0.05$).

3. Results

3.1. The roles of the lubricant on tribocorrosion degradation

The total mass loss measured after the tribocorrosion tests via VSI analysis is shown in Figure 1. It is observed that the presence of PBS in the solutions tends to lead to increased material loss. When the saline solutions are compared, PBS solution shows significantly higher mass loss than 0.9% NaCl solution. Additionally, 25% serum - PBS tends to show higher mass loss than 25% serum - DW, although the difference is not statistically significant. In general, a clear effect of the potential on the total material loss was not observed. In parallel, the study of the sample surface using VSI reveals that PBS leads to higher depth and width of the wear track (Figure 2), in concordance with the mass loss results shown in Figure 1. At the same time, depth and width of the wear track observed after tests in 25% serum – PBS are higher than those found in 25% serum – DW.

The effect previously observed, where PBS lead to increased degradation, is not as prominent in the case of the electrochemical losses (Figure 3 (a)), where only a slight tendency towards higher damage in the two PBS solutions can be seen. On the other hand, wear dominated losses (Figure 3 (b)) observed in PBS are significantly higher than those calculated for 0.9 % NaCl solution, in parallel with the total degradation losses. Wear losses also tend to increase in 25% serum – PBS in comparison to 25% serum – DW. The addition of serum to PBS (25% serum – PBS) leads to a significant reduction of wear dominated losses in comparison with PBS.

The increased in applied anodic over-potential showed a tendency to increase mass losses due to electrochemical processes. This is likely due to the increased oxidation kinetics at the higher applied over-potentials.

The relative weight of the electrochemical losses and mechanically dominated losses in each of the studied solutions is shown in Figure 4. It is observed that the contribution of the electrochemical losses to the total degradation losses varies depending on the electrolyte solution used. In the case of 0.9% NaCl solution electrochemical, reactions contributed to approximately 50% of the total material loss. When compared to PBS, material loss due to electrochemical processes decreased to around 20-25%. A slight reduction of the contribution to electrochemical losses were observed when serum containing lubricants were used. In this case, the percentage contribution of material loss due electrochemical losses in 25% serum – DW is around 40-45%. Whereas in 25% serum – PBS material loss due to corrosion related processes accounts for 35-40% of the total material lost during sliding.

The friction coefficient measured during the tribocorrosion tests is show in Figure 5. The presence of PBS in the solution leads to increased friction values. The highest friction coefficient was observed in the PBS solution. At the same time, 25% serum – PBS solution shows higher friction values than 25% serum – DW. In addition, serum containing solutions show decreased friction values when compared to the saline solutions.

SEM/EDX was used to analyse the sample surfaces (Figure 6). All test show clear abrasion marks along the wear track. A larger amount of deposits are found on the alloy surface after tribocorrosion tests in PBS solution (Figure 6 (b)) compared to 0.9% NaCl solution (Figure 6 (a)). Surfaces deposits were also observed for samples slid in serum containing lubricants. EDS analysis of the deposits found on the CoCrMo surface after tribocorrosion indicated that deposits were rich in P, Cr and O. Then slid in serum containing environments the addition of C and S were observed which will have originated from the organic species [12].

The analysis of the size of the particles formed during the tribocorrosion tests is shown in Figure 7. Both serum solutions (25% serum in DW and in PBS) and 0.9% NaCl solution show a mean particle size range of 150-200 nm. Whereas in the case of PBS, the mean particle range was 20-50 nm which may be an indication of microstructural changes occurring during the wear-corrosion tests due to variation of friction and shear stress at the interface.

3.2. The roles of the lubricant on repassivation kinetics

An example of the behaviour of the corrosion currents of the studied CoCrMo alloy when it was exposed to wear is shown in Figure 8. The first region reveals low current values due to the presence of a highly protective oxide film on the surface. The disruption of the passive film due to the onset of the tribological test causes a sudden increase of the current. A cyclic variation of current is observed due to the dynamic nature of de/repassivation as a result of the sinusoidal sliding velocity applied whereby periods of zero velocity will be experienced at the ends of the wear track. Once the tribological test is stopped, the current quickly decreases due to the reformation of the oxide layer. This last part of the curve is denoted as the repassivation phase. Two different exponential equations were fitted to the experimental data to study the repassivation phase. Least-squares method was used to fit the exponential equations to the experimental data. Firstly, a first order exponential decay was used according to Equation 3:

$$I(t) = I_1 \exp\left(\frac{-t}{\tau_1}\right) + I_2 \quad (3)$$

where I(t) represents the evolution of the corrosion current with time; t is the time in seconds; the maximum current of the curve is noted as I_1; the time constant that governs the exponential is noted as τ_1; and the remaining currents when the effect of the exponential diminishes are noted as I_2.

In addition to the first order exponential, a second order exponential decay was also fit to the experimental data, according to Equation (4):

$$I(t) = I_1 \exp\left(\frac{-t}{\tau_1}\right) + I_2 \exp\left(\frac{-t}{\tau_2}\right) + I_3 \quad (4)$$

where t is time in seconds; I_1 and I_2 are the maximum currents of the two exponential curves; τ_1 and τ_2 are the time constants that control each exponential decay; and I_3 is the current that remains when the effect of the two exponentials diminishes as time increases, which corresponds to the corrosion current in static conditions. A representation of each component of Equation (2) is shown in Figure 9.

A representative experimental repassivation curve of HC CoCrMo alloy in each of the studied solutions is shown in Figure 10. A comparison of the two curves fitted to the experimental data according to Equation (3) and Equation (4) is also shown. Values of the coefficient of determination (R^2) of each of the fitted curves are shown in Table 2. The first order exponential decay closely represents the experimental data at the beginning of the curve, for times lower than τ_1, and at the end of the curve, when the effect of the exponential is reduced. However, an underestimation of the currents is observed in the middle region, as seen in Figure 10.

The second order exponential equation represents the experimental data more accurately throughout the curve, and the underestimation of the current values was not observed in this case. It is also observed that R^2 values are higher in this case. A second order exponential decay represented the experimental data more closely than a first order exponential decay under the studied conditions.

The effect of each of the components of the second order exponential decay described by Equation (4) are also shown in Figure 10. It is observed that the first component, $I_1 \exp(-t/\tau_1)$, is dominant in the first part of the curve, where current rapidly drops towards values closer to passivity. After that, the repassivation rate is not as fast as in the previous stage, and current starts to decrease more slowly, dominated by the second component of the equation, $I_2 \exp(-t/\tau_2)$. Finally, more stable current values are reached around I_3, when the effect of the two first components of the exponential equation is reduced.

The peak currents observed when the alloy was subject to wear are shown in Figure 11. Lower peak currents are observed when serum was present in the solutions, suggesting a lubricating effect of proteins. It was also observed that higher applied anodic over-potentials results in higher peak currents. Time constants τ_1 and τ_2, obtained by fitting Equation (4) into the experimental data are shown in Figure 12. An effect of the potential on τ_1 is observed. Higher potential leads to lower values of τ_1, hence faster repassivation rates in the region governed by τ_1. The study of the effect of the electrolyte solution reveals higher τ_1 values in the case of 25% serum solution in distilled water, which indicates a slower drop of the currents in the first region of the repassivation. On the other hand, τ_1 shows similar values in the other three studied solutions. In the case of τ_2, no clear effect of potential or electrolyte solution is observed, showing similar values in all studied conditions.

4. Discussion

This study has investigated the roles of environment (i.e. lubricant) and electrochemical polarisation on the degradation mechanisms of CoCrMo alloy. It goes further to link the repassivation behaviour of the passive films with the simulated environment and resultant degradation mechanism and debris size distribution. The use of CoCrMo alloys in biomedical applications is still extensive despite the recent high profile issues associated with metal-on-metal total hip replacements [15]. In order to progress the current state of the art in metallic device innovation, it vital that a thorough understanding of the time-dependant and transient processes occurring at the metal interfaces are well understood; it is these processes that often limit the success of a medical device. From a pre-clinical assessment point of view, it is important to understand how simple changes in the environment and electrochemical conditions influence the resultant degradation processes.

4.1. Influence of the lubricant on the material loss mechanisms

The degradation of CoCrMo alloys under tribocorrosion conditions in simulated body fluids, and the effect of the chemical composition on the degradation of the material have been

investigated. The analysis of the total mass loss, shown in Figure 1, reveals that the presence of PBS in the electrolyte solution tends to increase the degradation of the alloy under the studied conditions, which is also confirmed by the 3D analysis of the geometry of the wear track (Figure 2). Previous studies have shown that negatively charged phosphates contained in PBS solutions have the ability to reduce corrosion currents in the absence of wear, by inhibiting the anodic reaction [8]. In the present work, samples are polarised and a potential in the passive range of the material is maintained before, during and after the tribological test. When the material is anodically polarised and the potential is kept stable, there is a continuous attraction of negatively charged species, which can then accumulate and enhance their effect on wear-corrosion degradation. The addition of 25v% of bovine calf serum to the PBS solution tends to lead to a reduction of the total loss in comparison to the PBS solution. On the other hand, the mass losses observed tend to be higher than those in 25% serum in distilled water. A competition between negatively charged proteins and phosphates to adsorb on the surface could be the cause behind the reduction on the effect of phosphates on the degradation of the alloy.

A simplified analysis of the total tribocorrosion losses is shown in Figures 3 and 4. The total loss measured during the study was divided in two components: 1) material loss due to pure corrosion (C) and wear enhance corrosion (C_w) calculated from electrochemical polarisation data and commonly noted as M_{chem} (Figure 3a) and 2) material loss due to pure wear (W) and wear enhanced corrosion (W_c) calculated via mass balance using gravimetric assessment and electrochemical data (Figure 3b). No statistically significant variations of mass loss due to $C+C_w$ were observed with increasing applied over potential for CoCrMo slid in 0.9% NaCl, PBS and 25% (v/v) Serum - PBS. An increase in the mass loss due to $C+C_w$ was observed between 0 and 0.2V although no significant difference was seen between 0.2 and 0.4V. At all applied anodic polarisations mass loss due to $C+C_w$ was lowest in 25% (v/v) Serum – DW, likely due to the decreased solution conductivity. Statistically significant differences in the material loss owing to ‘mechanical’ processes was seen. At all applied anodic over-potentials PBS was seen

to increase material loss from the CoCrMo surface. No obvious effect of applied over-potential was seen for any of the lubricants tested. The ratio between electrochemically dominated losses and mechanically dominated losses is also altered by the chemical composition of the media, as shown in Figure 4. The relative weight of electrochemical losses is ~ 50% in 0.9% NaCl solution, whereas it drops to values around 20-25% in PBS. This clear difference was not observed between the serum solutions, which indicates that proteins contained in serum may be limiting the effects of phosphates. The synergistic effect between wear and corrosion (i.e. C_w and W_c) was not isolated in this study and as such the 'mechanical' contributions ($W+W_c$) contain a mass loss contribution due to corrosion.

In addition to the effects of the composition of the solution on the wear and corrosion degradation of the CoCrMo alloy, the study of the coefficient of friction (Figure 5) confirms that the addition of PBS has an effect on the tribological performance of the material increasing not only wear loss but also friction coefficient. SEM/EDX analysis was performed to study the surface of the wear track after testing (Figure 6). When comparing the surface of the saline solutions, dark deposits on the surface of the CoCrMo tested in PBS solution were seen counter to the observations made for CoCrMo tested in 0.9%NaCl. The analysis of the composition revealed high amount of phosphorus in the deposits, which indicates that phosphates are depositing on the surface, leading to higher friction and higher wear. In the case of the serum solutions, dark deposits were found on both 25% serum – DW and 25% serum – PBS. Different species contained in the serum solutions can deposit on the surface of the sample, which can contain of phosphorus [12]. In the 25% serum – PBS solution, the species contained in serum and the phosphates from the PBS may be competing to adsorb on the surface, however, the presence of phosphorus in both of them makes it is difficult to differentiate the main source of the deposits.

Tribocorrosion degradation can lead to the release of metallic ions and metallic particles into the solution [5]. The size of the particles released was studied by Nanoparticle Tracker Analysis and the size distribution is shown in Figure 7. The predominant size range in 0.9% NaCl

solution and the two serum solutions rounds 150-200 nm, however, when tests are performed in PBS solution, the predominant size range drops to values around 20-50 nm. PBS solution does not only show higher mass loss and higher friction, but it also changes the size of the particles formed during the process.

The use of PBS leads to higher friction forces, therefore higher shear stresses on the surface, which may result in a refinement of the microstructure near the surface in contact with the counter surface. The formation of smaller structural grains as a results of tribological shear could be the cause of the reduction of the size of the released particles in the PBS solution, an observation that has been mooted by other researchers [22]. Whilst the clinical implications of these findings are not clear at this stage, this study highlights the sensitivity and importance of considering the testing methodologies and lubricants used for the preclinical testing of biomedical alloys. Furthermore, it is common place for biological assessment of 'wear debris' to be conducted on particulates derived from tests conducted in aseptic conditions using de-ionised water. This study raises further question on the suitability and validity of such approach when assessing medical devices pre-clinically.

4.2. The Influence of lubricant on the repassivation rates

Goldberg and Gilbert [20] studied the repassivation of a CoCrMo alloy using a scratch test apparatus with a stylus with a minor radius of 10 µm. In that study, the experimental data is fitted to a first order exponential decay. The authors propose a model, based on a previous model suggested by Ambrose [23], where the total repassivation current is described as the composition of the ionic dissolution current and the oxide film formation current, and both currents are defined as a function of the fraction of the surface covered by oxide, which is represented by θ, as shown in Equation 5:

$$I(t) = I_f + I_d = \frac{\delta \rho z F A_0}{M_w} \frac{d\theta}{dt} + j_{do} A_0 (1-\theta) \exp[\eta_d / b_a]$$

Where $\theta = 1 - \exp[-t/\tau]$ (5)

Film growth current (I_f) is defined by the authors as a function of a constant film thickness (δ), oxide film density (ρ), charge per cation (z), Faraday's constant (F), initial damaged area (A_0), molecular weight of the oxide film (M_w) and time (s). The dissolution current (I_d) is described assuming a Tafel-like behaviour where j_{do} is the exchange current density, η_d is the overpotential for the dissolution reaction and b_a is the Tafel slope for dissolution. In another investigation, Sun et al. [21] used a second order exponential equation to model the repassivation of a CoCrMo alloy. In that study, a micro-abrasion tester was used. The authors suggest that more complex damaged areas and limited diffusion of oxygen towards the surface can be some of the reasons for the differences of the obtained results.

In the present study, it was observed that a second order exponential equation described the current transients more closely than a first order exponential decay, as shown in Figure 10. The ball on plate configuration used in this study can lead to a larger and more complex damaged area, limiting the diffusion of oxygen towards the wear track, where the rate of oxygen consumption is higher due to the dissolution and repassivation processes. These observations are parallel with the results shown by Sun and co-authors [21]. The limited diffusion of oxygen can slow down the repassivation process, leading to an underestimation of current values, observed in Figure 10, when the first order exponential equation is used (dashed line).

Passive film growth has been studied by several authors over the years [23-26]. Jemmely and co-authors [26] modelled the repassivation of an iron-chromium alloy in sulphuric acid considering two repassivation models, a surface coverage model, where the oxide film grows to cover the exposed area; and a film growth model, where the oxide film uniformly grows and thickens on the surface of the metal. The assumption that no metal dissolution occurs is considered in the two models proposed by the authors.

The two model approach described by Jemmely et al. [26] can be used to rationalise the good correlation between a second order exponential equation and the experimental data obtained in this work. The two exponential components of Equation (4) can be defined as $I^{coverage}$ and

$I^{thickening}$. The remaining currents when the material is completely repassivated can be denoted as $I^{passive}$, resulting in Equation (6).

$$I(t) = I^{coverage}(t) + I^{thickening}(t) + I^{passive}(t) \quad (6)$$

On the other hand, in parallel with the model proposed by Goldberg and Gilbert[20] (Equation (5)), it can be assumed that the currents measured during the tribocorrosion test are a combination of dissolution currents and film formation currents; therefore currents taking place in the coverage, thickening and passive phases (Eq. (6)) will be a composition of dissolution (I_d) and film formation (I_f) currents, as shown in Equation (7).

$$I(t) = \left(I_f^{coverage}(t) + I_d^{coverage}(t)\right) + \left(I_f^{thickening}(t) + I_d^{thickening}(t)\right) + \left(I_f^{passive}(t) + I_d^{passive}(t)\right) \quad (7)$$

At the beginning of the repassivation process, mechanical damage has removed the passive film leaving a portion of the area depassivated. In these zones of material, the base alloy is exposed to the corrosive media and the reformation of the oxide layer on the active areas dominates the corrosion currents. The exposure of the base material leads to increased electrochemical reactivity, enhancing the dissolution of the metal (Figure 13a). The fraction of the surface of base material (A) that is exposed to the corrosive media, noted by $\theta_A^{coverage}$, will determine the rate of the electrochemical reactions. The combination of Eq. (5) and the coverage component of Eq. (7) leads to the definition of $I^{coverage}$ shown in Equation (8).

$$I^{coverage}(t) = \left(I_f^{coverage} + I_d^{coverage}\right) = \frac{\rho z F}{M_w}\delta^{coverage} A_0 \frac{d\theta_A^{coverage}}{dt} + j_{do}^{coverage} \exp\left[\eta_d^{coverage} / b_a^{coverage}\right] A_0 (1 - \theta_A^{coverage})$$

$$\text{where } \theta_A^{coverage}(t) = 1 - \exp\left[-t / \tau_{coverage}\right] \quad (8)$$

Once most of the surface has been covered by the reformed oxide film, the base alloy is no longer exposed and dissolution is largely reduced. The repassivation reaction is dominated by the growth of the thickness of the passive layer, which further limits dissolution and leads to a reduction of the corrosion current (Figure 13b). The thickness of the oxide layer controls the parameters that govern the rate of the reactions, affecting both dissolution and oxide film

formation currents. The growth of the film thickness (δ) is governed by the parameter $\theta_\delta^{thickening}$. The combination of Equation (5) and Equation (8) leads to Equation (9).

$$I^{thickening}(t) = \left(I_f^{thickening} + I_d^{thickening}\right) = \frac{\rho z F}{M_w}\delta^{thickening} A_0 \frac{d\theta_\delta^{thickening}}{dt} + j_{do}^{thickening} \exp\left[\eta_d^{thickening} / b_a^{thickening}\right] A_0 (1-\theta_\delta^{thickening})$$

$$\text{where } \theta_\delta^{thickening}(t) = 1 - \exp\left[-t/\tau_{thickening}\right] \quad (9)$$

Once the passive film is completely rebuilt, the current values reach values similar to those observed before the tribological test was started. The rate of the reactions is largely reduced and the diffusion of metal ions through the oxide film dominates the corrosion currents [9].

The first time constant τ_1, which corresponds to the defined $\tau_{coverage}$, is shown in Figure 12. It is observed that $\tau_{coverage}$ tends to be lower at higher potentials, indicating a faster repassivation rate. The higher reactivity under these conditions enhances the reformation of the oxide layer but also the dissolution of the base metal, which leads to higher peak currents (Figure 11). It is also observed that $\tau_{coverage}$ is higher in the case of 25% serum in distilled water in the two studied alloys due to the lower conductivity of the solution. The second time constant τ_2, which is equivalent to $\tau_{thickening}$, is shown in Figure 13. In this case, the surface is already covered by a highly protective oxide layer and the effect of the potential is not noticeable, suggesting that the dissolution reaction is not dominant at this stage but it is the reformation of the passive film which dominates the reactions. In addition, differences between electrolyte solutions are not observed in this case. The conductivity of the media does not have a strong effect in this repassivation stage because dissolution currents are diminished once the first layers of oxide film cover the surface.

5. Conclusions

The effect of the chemical composition of the media on the tribocorrosion behaviour of a CoCrMo alloy has been investigated. The main conclusions that can be drawn from this study are:

- PBS containing solutions tend to show higher mass loss than the solutions prepared with distilled water. This is especially noticeable in the case of PBS solution, which shows significantly higher mass loss than that of 0.9% NaCl.
- Proteins from the serum and phosphates from PBS tend to compete to adsorb on the surface reducing the mass loss observed in 25% serum – PBS in comparison to PBS solution.
- The presence of phosphates in the solution does not clearly affect the losses caused by electrochemical reactions. The larger effect is observed on the losses dominated by mechanical phenomena.
- Formation of phosphate deposits on the surface of the samples is observed after testing. The formation of such deposits can have an effect on the contact increasing wear and friction.
- The mean particulate size decreased in PBS when compared to other lubricants. This compliments higher wear and friction measurements and suggest that phosphates influence the acting abrasive wear mechanism at the interface.
- The degradation of the studied CoCrMo alloys due to tribocorrosion phenomena shows a great dependence on the chemical composition of the media and should be considered in all pre-clinical testing.

6. References

[1] Sweeney CA, O'Brien B, McHugh PE, Leen SB. Experimental characterisation for micromechanical modelling of CoCr stent fatigue. Biomaterials 2014;35:36-48.

[2] Hedberg YS, Qian B, Shen Z, Virtanen S, Odnevall Wallinder I. In vitro biocompatibility of CoCrMo dental alloys fabricated by selective laser melting. Dent Mater 2014;30:525-34.

[3] Saikko V, Ahlroos T, Revitzer H, Ryti O, Kuosmanen P. The effect of acetabular cup position on wear of a large-diameter metal-on-metal prosthesis studied with a hip joint simulator. Tribol Int 2013;60:70-6.

[4] Milošev I, Strehblow H. The composition of the surface passive film formed on CoCrMo alloy in simulated physiological solution. Electrochim Acta 2003;48:2767-74.

[5] Rituerto Sin J, Hu X, Emami N. Tribology, corrosion and tribocorrosion of metal on metal implants. Trib Mater Surf & Interfaces 2013;7:1-12.

[6] Virtanen S, Milošev I, Gomez-Barrena E, Trebše R, Salo J, Konttinen YT. Special modes of corrosion under physiological and simulated physiological conditions. Acta Biomaterialia 2008;4:468-76.

[7] Espallargas N, Torres C, Muñoz AI. A metal ion release study of CoCrMo exposed to corrosion and tribocorrosion conditions in simulated body fluids. Wear 2015.

[8] Igual Muñoz A, Mischler S. Interactive effects of albumin and phosphate ions on the corrosion of CoCrMo implant alloy. J Electrochem Soc 2007;154:562-70.

[9] Heuberger MP, Widmer MR, Zobeley E, Glockshuber R, Spencer ND. Protein-mediated boundary lubrication in arthroplasty. Biomaterials 2005;26:1165-73.

[10] Yan Y, Neville A, Dowson D, Williams S. Tribocorrosion in implants: assessing high carbon and low carbon Co--Cr--Mo alloys by in situ electrochemical measurements. Tribol Int 2006;39:1509-17.

[11] Mazzucco D, Spector M. The John Charnley Award paper: the role of joint fluid in the tribology of total joint arthroplasty. Clin Orthop 2004;429:17-32.

[12] Wimmer MA, Sprecher C, Hauert R, T\ager G, Fischer A. Tribochemical reaction on metal-on-metal hip joint bearings: a comparison between in-vitro and in-vivo results. Wear 2003;255:1007-14.

[13] Yan Y, Neville A, Dowson D, Williams S, Fisher J. Tribofilm formation in biotribocorrosion--does it regulate ion release in metal-on-metal artificial hip joints? Proc.Inst.Mech.Eng.J J.Eng.Tribol. 2010;224:997-1006.

[14] Hesketh J, Ward M, Dowson D, Neville A. The composition of tribofilms produced on metal-on-metal hip bearings. Biomaterials 2014;35:2113-9.

[15] Liao Y, Pourzal R, Wimmer MA, Jacobs JJ, Fischer A, Marks LD. Graphitic Tribological Layers in Metal-on-Metal Hip Replacements. Science 2011};334}:1687-1690}.

[16] Narayan RJ. ASM Handbook, Volume 23 - Materials for Medical Devices. : ASM international, 2012.

[17] Metikoš-Huković M, Pilić Z, Babić R, Omanović D. Influence of alloying elements on the corrosion stability of CoCrMo implant alloy in Hank's solution. Acta Biomaterialia 2006;2:693-700.

[18] Stack MM, Rodling J, Mathew MT, Jawan H, Huang W, Park G et al. Micro-abrasion--corrosion of a Co--Cr/UHMWPE couple in Ringer's solution: An approach to construction of mechanism and synergism maps for application to bio-implants. Wear 2010;269:376-82.

[19] Lewis AC, Kilburn MR, Papageorgiou I, Allen GC, Case CP. Effect of synovial fluid, phosphate-buffered saline solution, and water on the dissolution and corrosion properties of CoCrMo alloys as used in orthopedic implants. J Biomed Mater Res A 2005;73A:456-67.

[20] Rituerto Sin J, Neville A, Emami N. Corrosion and tribocorrosion of hafnium in simulated body fluids. Journal of Biomedical Materials Research Part B: Applied Biomaterials 2014;102:1157-64.

[21] Watson S, Friedersdorf F, Madsen B, Cramer S. Methods of measuring wear-corrosion synergism. Wear 1995;181:476-84.

[22] Ahmed R, de Villiers Lovelock HL, Faisal NH, Davies S. Structure–property relationships in a CoCrMo alloy at micro and nano-scales. Trib Int 2014;80:98-114.

7. Figures

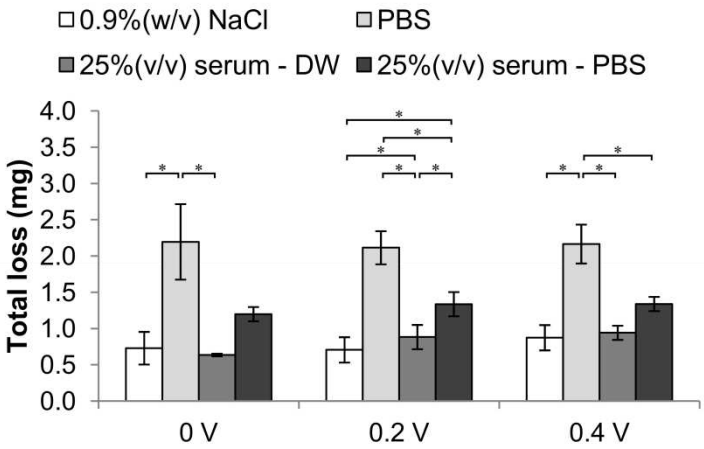

Figure 1 The total mass loss from CoCrMo plate via VSI measurement at 0, 0.2 and 0.4V vs Ag/AgCl. Mass loss data shows higher degradation in the PBS-based solutions.* shows were statistically significant differences in mass loss data were seen ($P<0.05$)

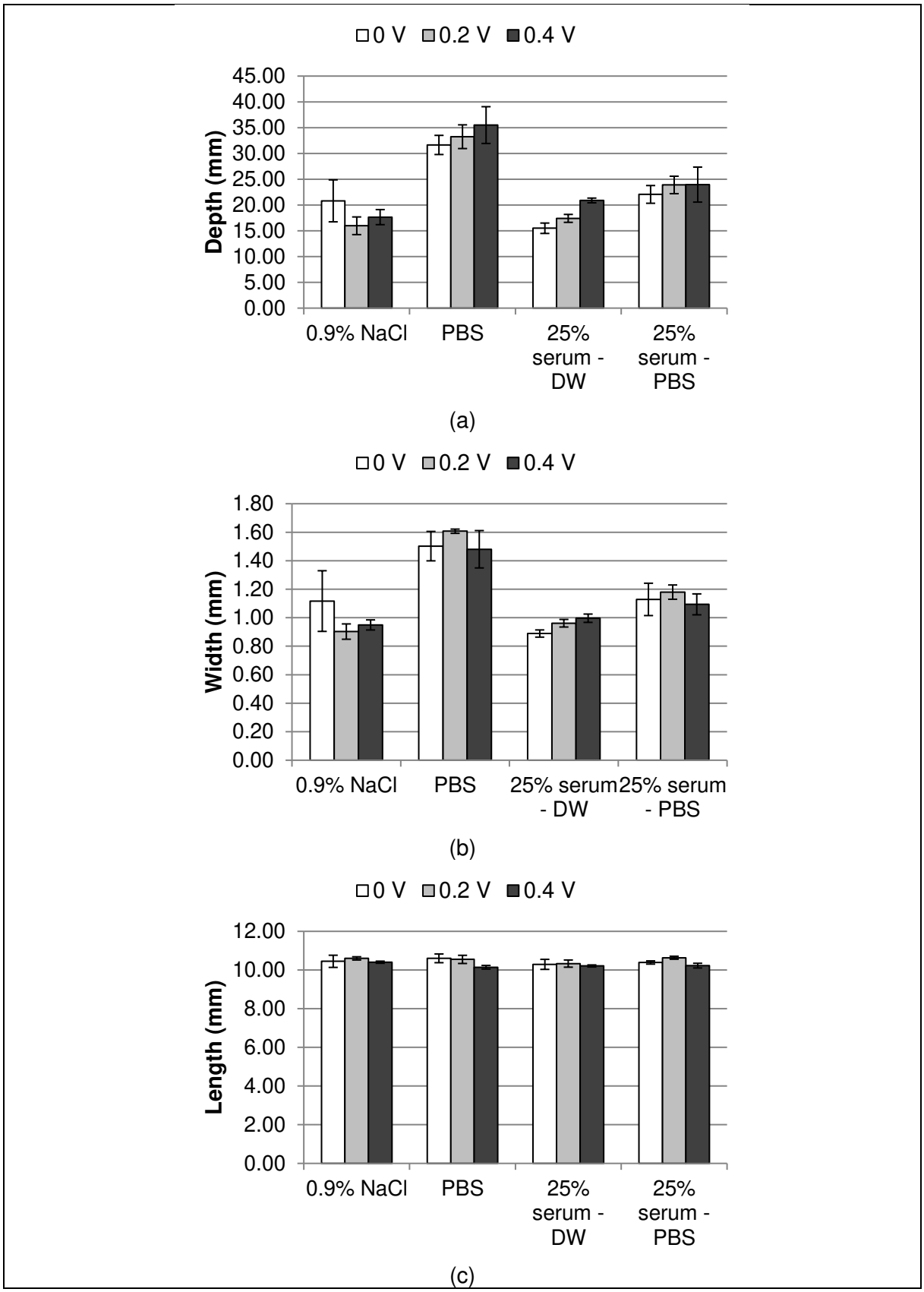

Figure 2 Analysis of the depth, width and length of the wear track formed during the tribocorrosion tests.

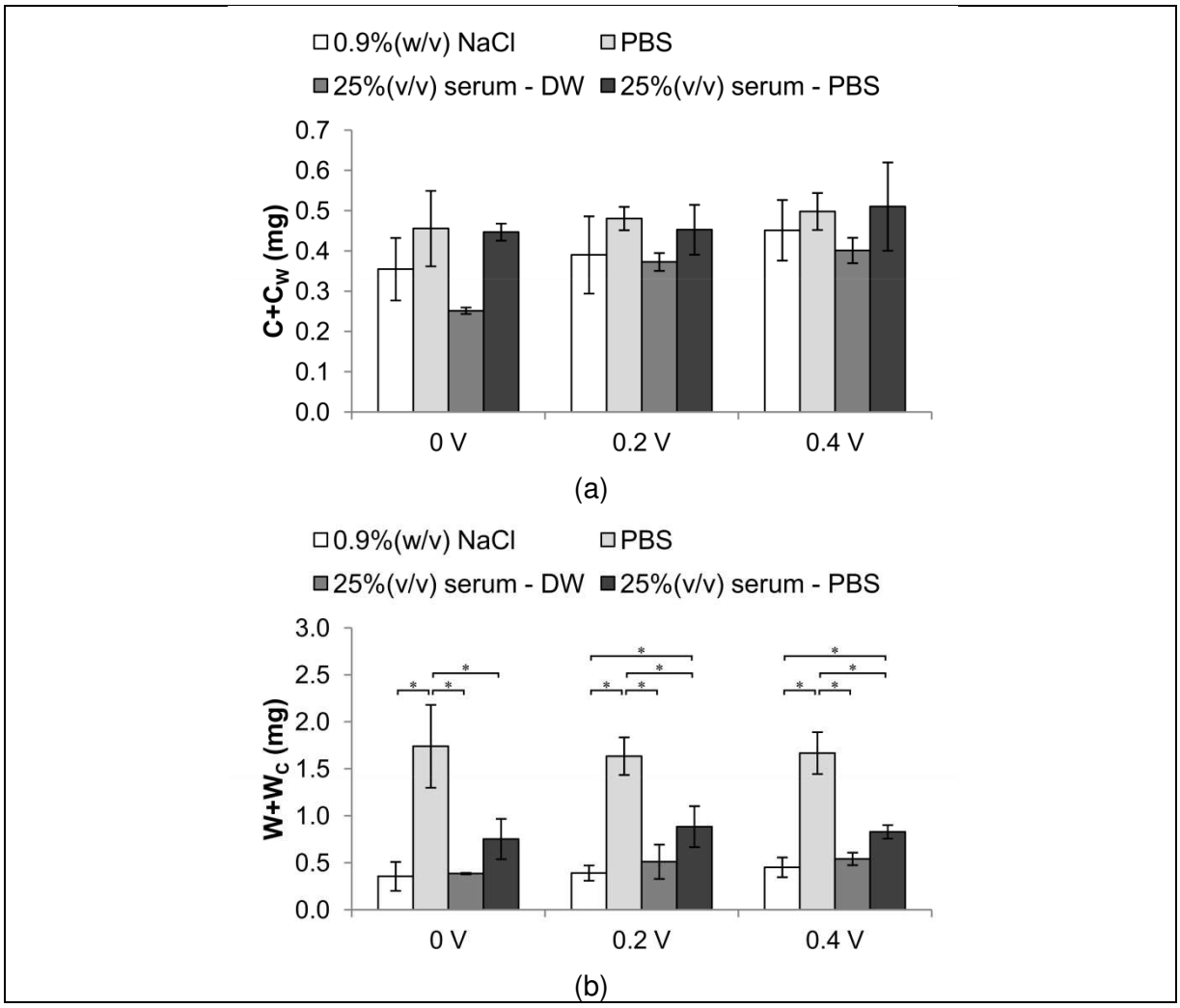

Figure 3 The total loss has been decomposed in electrochemical losses and mechanical losses.

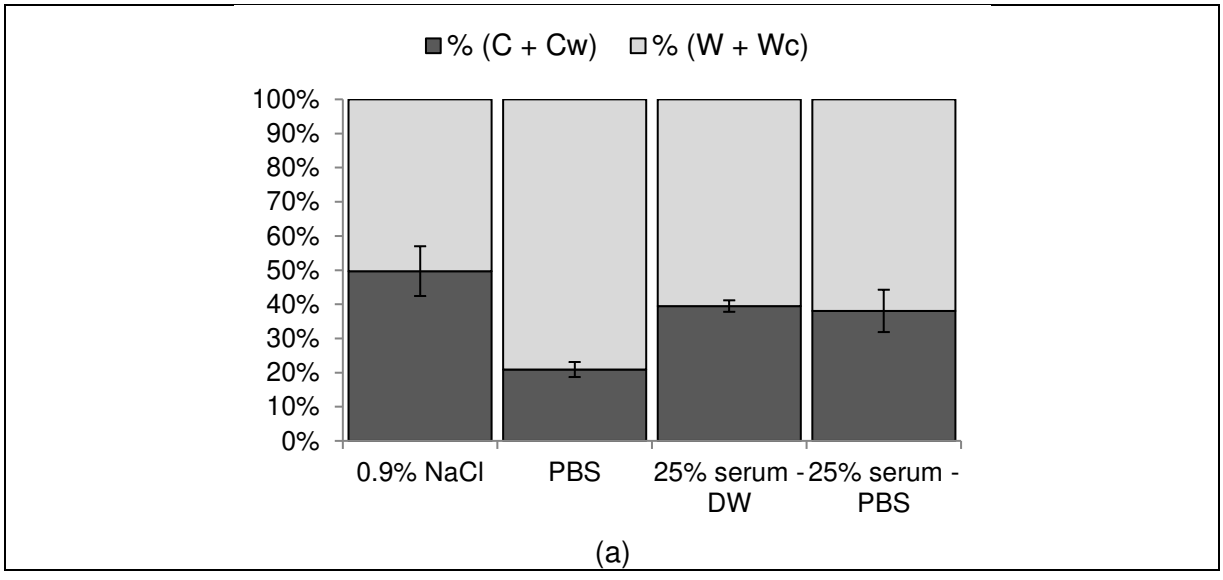

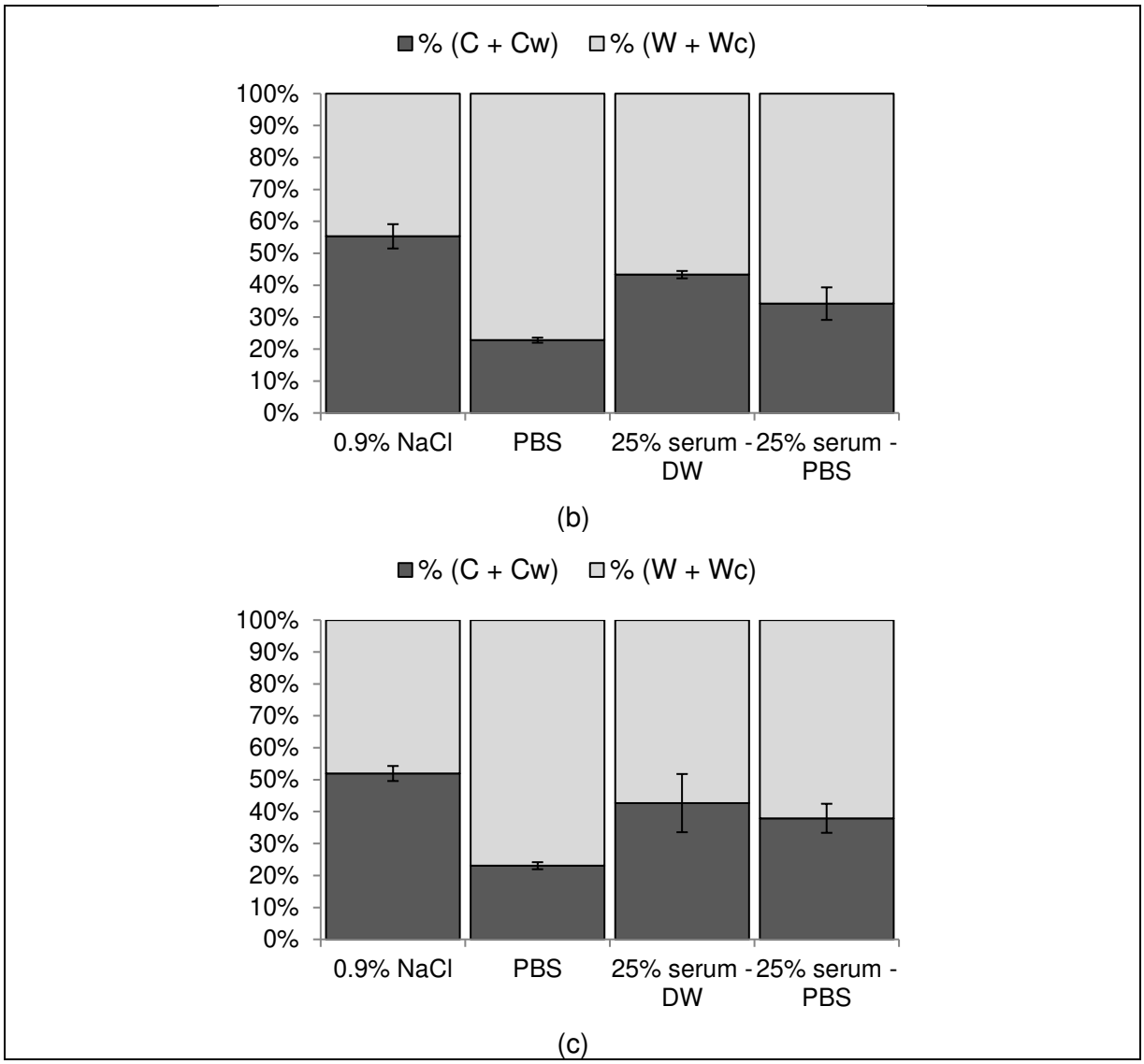

Figure 4 Analysis of the contribution of the electrochemical losses and mechanical losses to the total degradation losses of the material at a) 0, b) 0.2 and c) 0.4 V vs Ag/AgCl.

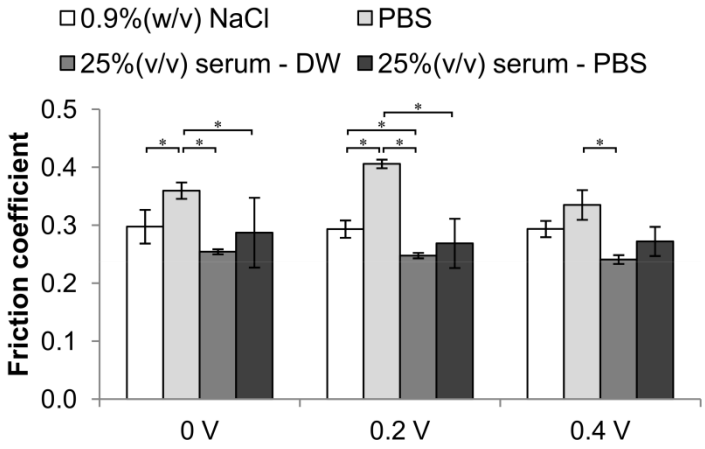

Figure 5 Average coefficient of friction measured during the tribocorrosion tests at the applied over-potentials studied .* shows were statistically significant differences in mass loss data were seen ($P<0.05$)

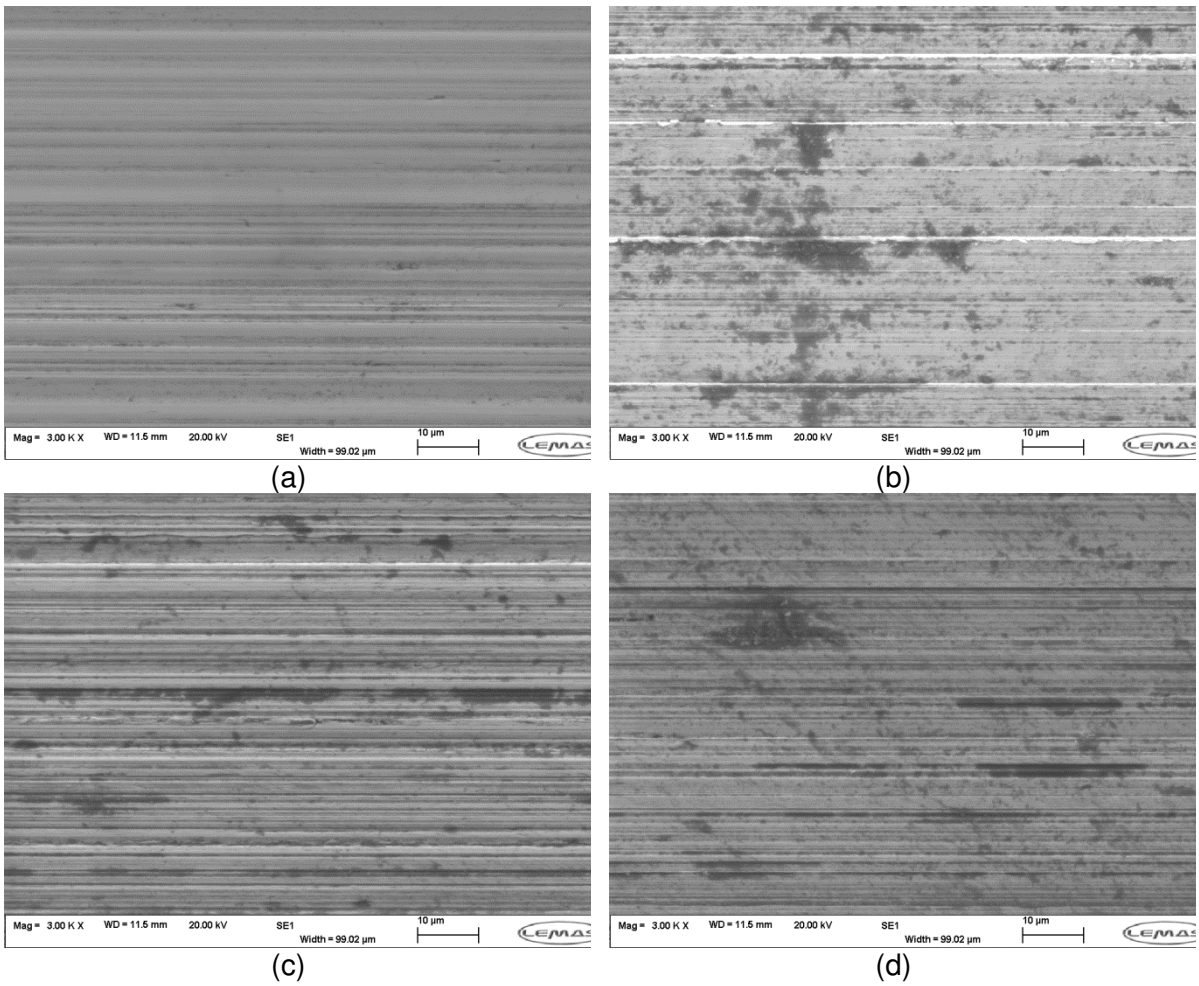

Figure 6 SEM images of the wear track after tribocorrosion tests performed at 0V in 0.9% NaCl (a), PBS (B), 25% serum – DW (c) and 25% serum – PBS.

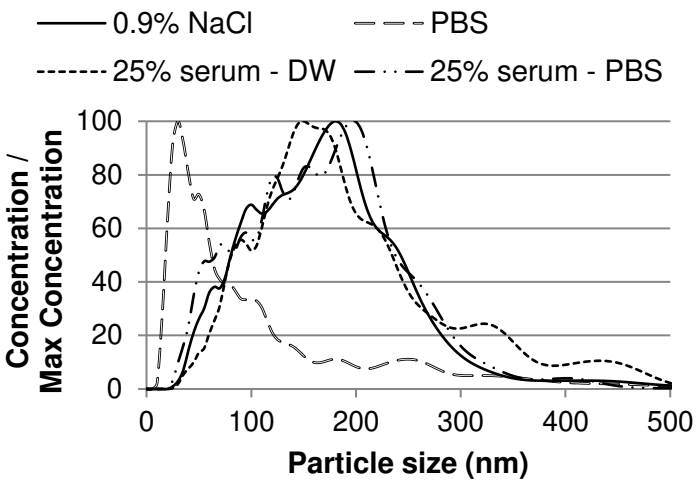

Figure 7 Analysis of the particle size of the wear debris.

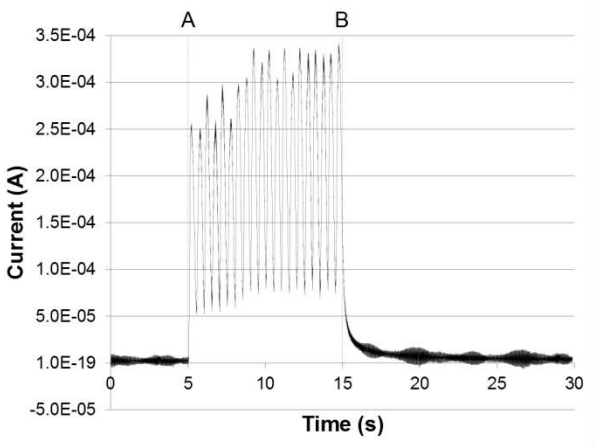

Figure 8 The measured currents increase at A, when the tribological test is started. The mechanical damage is stopped at B, as a consequence current drops towards values similar to those observed before A, indicating the effective reformation of the passive layer.

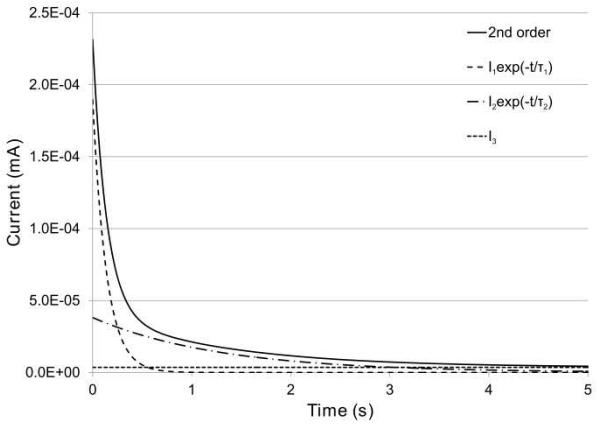

Figure 9 The second order exponential decay is a composition of the three equations shown. Each equation is dominant in one phase of the curve.

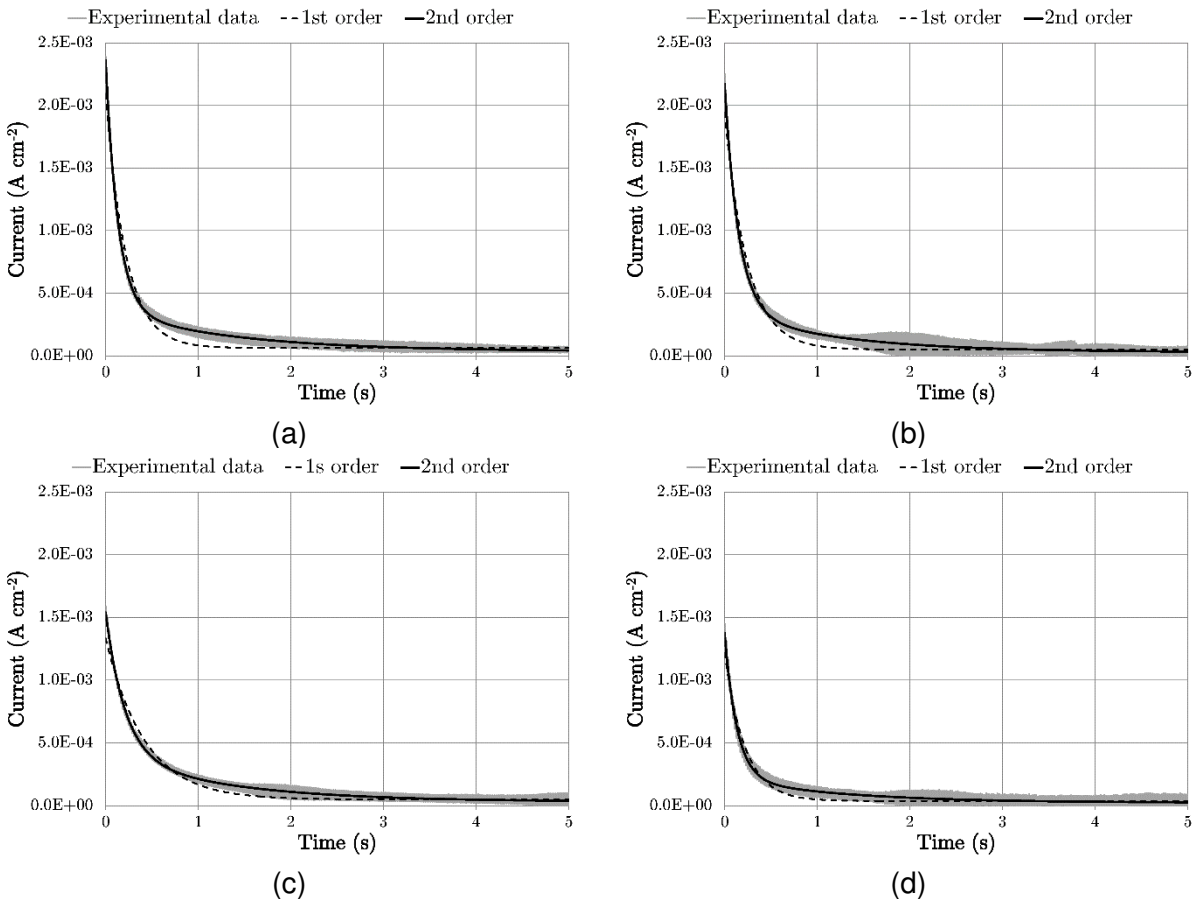

Figure 10 First order (dashed line) and second order (solid line) exponential equations fitted to the experimental repassivation data (gray line).

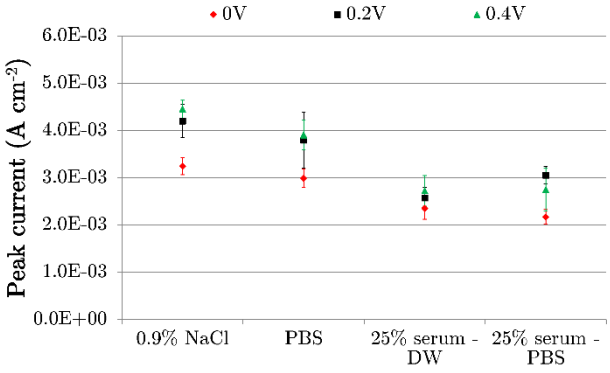

Figure 11 Peak currents measured when the material was subject to the tribological test.

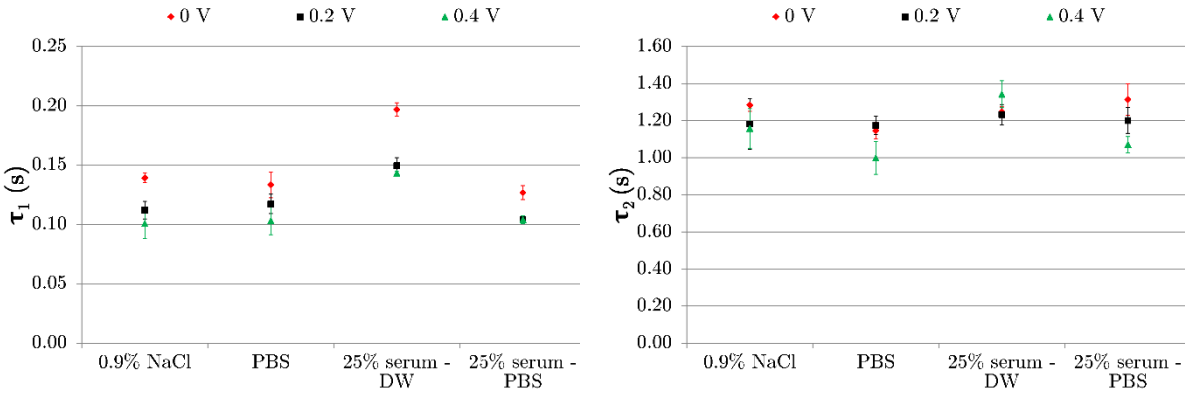

Figure 12 Effect of potential and solution on time constant τ_1 (a) and time constant τ_2.

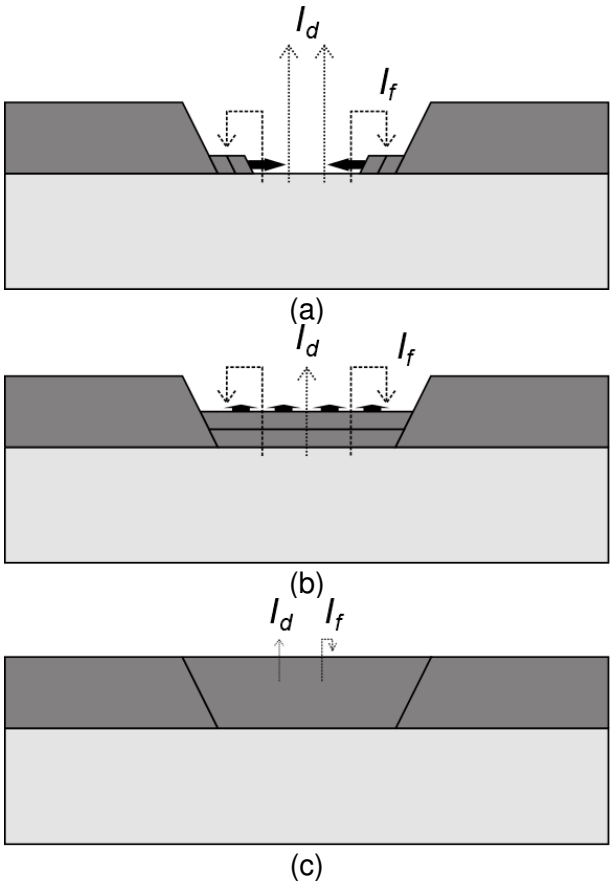

Figure 13 Schematic representation of the phases of repassivation process. In the coverage phase (a), the exposure of the base material allows higher dissolution currents. In the thickening phase (b), the reformed oxide film grows and its thickness increases, limiting dissolution. Once the oxide film has been completely reformed (c), corrosion currents are largely reduced.

8. Tables

Table 1 Summary of the solutions studied.

Notation	Preparation
0.9%NaCl	0.9 wt% NaCl 99.1 wt% distilled water
PBS	Phosphate Buffered Saline
25% serum – DW	25 v% bovine calf serum 75 v% distilled water
25% serum – PBS	25 v% bovine calf serum 75 v% phosphate buffered saline

Table 1 Coefficient of determination R^2 of the fitting methods studied.

	0.9% NaCl	PBS	25% serum - DW	25% serum - PBS
1st order – least squares	0.93 ± 0.02	0.87 ± 0.05	0.93 ± 0.01	0.86 ± 0.02
2nd order – least squares	0.97 ± 0.01	0.95 ± 0.01	0.97 ± 0.01	0.93 ± 0.03
±: Standard deviation				